Available online at www.sciencedirect.com
SCIENCE DIRECT®
Brain Research 1001 (2004) 108–117
BRAIN RESEARCH
www.elsevier.com/locate/brainres

Research report

Expression of the iron transporter ferroportin in synaptic vesicles and the blood–brain barrier

Laura Jui-chen Wu[a,b], A.G. Miriam Leenders[c], Sharon Cooperman[a], Esther Meyron-Holtz[a], Sophia Smith[a], William Land[a], Robert Y.L. Tsai[d], Urs V. Berger[e], Zu-Hang Sheng[c], Tracey A. Rouault[a,*]

[a] *Cell Biology and Metabolism Branch, National Institute of Child Health and Human Development, Bldg. 18T, Room 101, NICHD, Bethesda, MD, 20892, USA*
[b] *Chang Gung Memorial Hospital, Taiwan*
[c] *Synaptic Function Unit, National Institute of Neurological Disorders and Stroke, Bethesda, MD, USA*
[d] *Laboratory of Molecular Biology, National Institute of Neurological Disorders and Stroke, Bethesda, MD, USA*
[e] *UB-In Situ, Natick, MA, USA*

Accepted 16 October 2003

Abstract

Iron homeostasis in the mammalian brain is an important and poorly understood subject. Transferrin-bound iron enters the endothelial cells of the blood–brain barrier from the systemic circulation, and iron subsequently dissociates from transferrin to enter brain parenchyma by an unknown mechanism. In recent years, several iron transporters, including the iron importer DMT1 (Ireg1, MTP, DCT1) and the iron exporter ferroportin (SLC11A3, Ireg, MTP1) have been cloned and characterized. To better understand brain iron homeostasis, we have characterized the distribution of ferroportin, the presumed intestinal iron exporter, and have evaluated its potential role in regulation of iron homeostasis in the central nervous system. We discovered using in situ hybridization and immunohistochemistry that ferroportin is expressed in the endothelial cells of the blood–brain barrier, in neurons, oligodendrocytes, astrocytes, and the choroid plexus and ependymal cells. In addition, we discovered using techniques of immunoelectron microscopy and biochemical purification of synaptic vesicles that ferroportin is associated with synaptic vesicles. In the blood–brain barrier, it is likely that ferroportin serves as a molecular transporter of iron on the abluminal membrane of polarized endothelial cells. The role of ferroportin in synaptic vesicles is unknown, but its presence at that site may prove to be of great importance in neuronal iron toxicity. The widespread representation of ferroportin at sites such as the blood–brain barrier and synaptic vesicles raises the possibility that trafficking of elemental iron may be instrumental in the distribution of iron in the central nervous system.
Published by Elsevier B.V.

Theme: Cellular and molecular biology
Topic: Blood–brain barrier

Keywords: Iron transport; Synaptic vesicles; Endothelial transport; Neurodegeneration

1. Introduction

Iron is an essential element for normal cellular functions. Many enzymes in the electron transport chain, including cytochromes *a*, *b*, and *c*, and cytochrome oxidase, use iron as a cofactor for adenosine triphosphate (ATP) synthesis [11]. Iron also plays specific roles in the central nervous system (CNS). It is involved in myelin formation [7], as well as in the production of several neurotransmitters such as dopamine [19], norepinephrine and serotonin [7], and generation of GABAergic activity [16]. In addition, iron overload is implicated as a cause of neuronal death [3]. Abnormally high levels of iron in the brain have been demonstrated in a number of neurodegenerative disorders, including NBIA 1 disease (formerly known as Hallervorden-Spatz syndrome) [13], Parkinson's disease [3], autosomal recessive juvenile parkinsonism [25], multiple system atrophy [8], Alzheimer's disease [24] and Friedreich's ataxia [28].

* Corresponding author. Tel.: +1-301-496-7060; fax: +1-301-402-0078.
E-mail address: trou@helix.nih.gov (T.A. Rouault).

0006-8993/$ - see front matter. Published by Elsevier B.V.
doi:10.1016/j.brainres.2003.10.066

Despite the importance of iron for normal brain function, iron homeostasis in the CNS is still not well understood (reviewed in Ref. [20]). Iron preferentially accumulates in the striatum of aging animals, but the causes and significance of iron accumulation remain unclear [17]. Although much remains to be learned about the mechanisms responsible for iron uptake, transport, and export across the blood–brain-barrier (BBB) and within brain parenchyma, the recent identification and characterization of several membrane iron transporter proteins may provide new insights into these processes.

Prior studies of the iron importer DMT1 and iron exporter ferroportin 1 have demonstrated their importance in transport of iron across the duodenal mucosa and in iron homeostasis (reviewed in Ref. [2]). In the duodenal epithelium, DMT1 localizes to the apical membrane [6] where it mediates uptake of iron from the intestinal lumen, whereas ferroportin is present mainly in the basolateral membrane [9], where it is presumed to export elemental iron to the circulation. The ability of these two proteins to import and export iron across the plasma membrane has also been demonstrated in Xenopus oocytes [12] and cultured mammalian cells [1]. DMT1 transcripts have been detected by in situ hybridization in the choroid plexus and in neurons throughout the CNS. Ferroportin has previously been detected in pyramidal neurons and cerebellar Purkinje cells, but not in the choroid plexus or blood–brain barrier [5].

In mammalian cells, there are two cytosolic proteins, iron-regulatory proteins 1 and 2 (IRP1 and IRP2), that regulate expression of iron metabolism proteins, such as ferritin and transferrin receptor, by binding to a RNA stem loops known as iron-responsive elements (IREs) within transcripts of those proteins (reviewed in [21,22]. Clearly IRP2 has an important role in CNS iron metabolism, as evidenced by the fact that IRP2 −/− mice iron accumulate iron in characteristic regions of the brain that undergo neurodegeneration [15]. Ferroportin transcripts contain an IRE within the 5′ UTR, but the regulation of ferroportin through IRPs is incompletely understood [1]. Evaluation of ferroportin regulation and expression in the IRP2 −/− animal model therefore has the potential to provide insight into the mechanisms by which neurons regulate iron homeostasis.

In this study, we analyzed the distribution of ferroportin in the CNS of wild type and IRP2 −/− mice, and compared its expression levels in iron overload or depletion paradigms. We also discovered that ferroportin is expressed in synaptic vesicles, which may suggest a role of ferroportin in the regulation of neurotransmitter synthesis and/or synaptic function by iron.

2. Material and methods

2.1. Antibodies

Antibodies were raised against multiple antigenetic peptides (MAPs) [27] as previously described [15], including the mouse ferroportin 1 peptide sequence, aa 165–181 (ENRSRLADMNATIRRID, MAP23) or aa 240–258 (KVEESELKQLTSPKDTEPK, MAP 24) or aa 432–447 (EMHMSNMSNVHEMSTK, MAP 25). Anti-MAP antibodies were purified using affinity chromatography columns made by coupling the MAP antigen to cyanogen-bromide-activated Sepharose CL-4B.

2.2. Immunohistochemical studies

Mice of various genotypes and dietary treatments were intracardially perfused, post-fixed in formalin, embedded in paraffin and sectioned as described previously [15]. Non-specific binding was blocked with 10% goat serum and 0.3% Triton ×100 in 1× PBS for one hour at RT. Subsequently, these sections were incubated with antiMAP antibodies to ferroportin (5 μg/ml) in blocking buffer over night at 4 °C. The slides were washed with 1X PBS and incubated with the secondary antibody biotinylated antirabbit IgG (1: 1000, Vector Laboratories) followed by Avidin Biotin Complex labeled with horseradish peroxidase (ABC Elite kit, Vector Laboratories). HRP was visualized using the substrate diaminobenzidine (DAB, Vector Laboratories) with incubation for 5 min at RT. Peptide competitions were used as negative control. Doublelabeling immunofluorescence studies were carried out by incubating the brain sections with primary antibody to ferroportin and primary antibodies to neuronal nuclei (Neu N, mouse monoclonal antibody 1:100, Chemicon, CA), to astrocytes (GFAP, mouse monoclonal antibody 1:100) and to oligodendrocytes (CNPase, mouse monoclonal antibody 1:100) respectively followed by incubation with fluorconjugated secondary antibodies against rabbit or mouse IgG.

2.3. In situ analysis

Non-isotopic in situ hybridization was performed using digoxigenin (DIG)-labeled cRNA probes and alkaline phosphatase (AP) detection as described [4]. Briefly, cryostat sections of fresh frozen brain were cut at 10-μm thickness, fixed in 4% paraformaldehyde and acetylated. Hybridization was performed in slide mailers by total immersion in hybridization buffer that contained 50% formamide, 5× SSC, 2% blocking reagent (Roche Applied Science, Indianapolis, IN), 0.02% SDS, 0.1% sarcosine, and approximately 100 ng/ml of cRNA probe. Sections were hybridized at 68 °C over 72 h with the full-length mouse ferroportin probe (3kb) that had been alkali-hydrolyzed to around 500 bases in length. Washing steps included incubations in 2× SSC and 0.2× SSC at 68 °C. Sections were incubated at room temperature in 1% blocking reagent in maleic acid buffer, then in AP-conjugated anti-digoxigenin Fab fragments (1:5000 dilution, Roche), and developed overnight with BCIP/NBT substrate (Kierkegard and Perry Laboratories, Gaithersburg, MD). Sections were rinsed several times in 100 mM Tris, 150 mM NaCl, 20 mM EDTA pH 9.5, and

coverslipped with glycerol gelatin (Sigma). Control sections were incubated in an identical concentration of the sense probe transcript. Some slides were double-stained after the in situ hybridization procedure with a rabbit anti-GFAP antibody (DAKO) to examine expression in astrocytes. The anti-GFAP antibodies were visualized using a CY3-labeled secondary antibody.

2.4. Northern analysis

Total RNA was isolated from various mouse brain tissues using Trizol reagent (Life Technologies). Five micrograms total RNA were separated in 4% formaldehyde/1.2% agarose gels and transferred to a Nylon membrane. ^{32}P-labelled ferroportin probe was synthesized using random primer kit. Hybridization and washing conditions were as described previously, and transferrin receptor mRNA was detected as previously described [15].

2.5. Western blot

Western blot experiments were carried out as previously described [15]. In short, proteins were extracted in lysis buffer (0.125 M Tris, pH 6.8, 70 mM sodium dodecyl sulfate, 2% Glycerol, 10 μg/ml leupeptin, 10 μg/ml aprotinin, 10 μg/ml AEBSF). Samples were sonicated and assayed for protein concentration by BCA protein assay. 50 μg of protein was mixed with an equal volume of 4 × sample-loading buffer (0.5 M Tris, pH 6.8, 10% glycerol, 2% SDS, 0.7 M β-mercaptoethanol and 0.05% bromophenol blue), and fractionated in an 8% SDS acrylamide gel and transferred to a nitrocellulose membrane. The membrane was blocked with 5% non-fat milk in PBS and incubated with an antibody directed against ferroportin or DMT1. The membrane was stained with a horse-radish peroxidase-conjugated goat anti-rabbit IgG antibody (1:5000 dilution) and developed using enhanced chemiluminescence (ECL kit, Pierce).

2.6. Pre-embedding electron microscopic immunocytochemistry

Brain sections or cultured cells were fixed with 4% paraformaldehyde in 0.1 M phosphate buffer at pH 7.4 for 45 min, washed with buffer, permeabilized with 0.1% saponin and blocked with 5% normal goat serum in 1 × PBS for 1 h. They were then incubated with the primary antibody for 1 h, washed, incubated with the secondary antibody conjugated to gold (Nanogold, Nanoprobes, Yaphank, NY) for 1 h, washed, and fixed with 2% glutaraldehyde in 1 × PBS for 30 min. Samples were then washed and silver enhanced (HQ silver enhancement kit, Nanoprobes), treated with 0.2% osmium tetroxide in buffer for 30 min, 0.5% uranyl acetate for 30–60 min or overnight, washed, dehydrated in ethanol and finally embedded in epoxy resins and sectioned conventionally.

2.7. Synaptosomal preparations

Synaptosomes from rat brain were prepared from 3 week old rats maintained on a normal rodent chow diet by differential and discontinuous Percoll gradient centrifugation [10,23], and subcellular fractions were isolated on sucrose gradients as previously described [14]. Eight rat brains from three-week old animals maintained on normal mouse chow were processed for synaptosome preps. Briefly, after Percoll-sucrose gradient centrifugation, the synaptosomes were washed once in medium M (0.32 M sucrose, 1 mM K_2HPO_4, 0.1 mM EDTA [pH 7.5]), resuspended and homogenized in medium L (1 mM K_2HPO_4, 0.1 mM EDTA [pH 8.0]), and incubated at 4 °C for 1 h. The

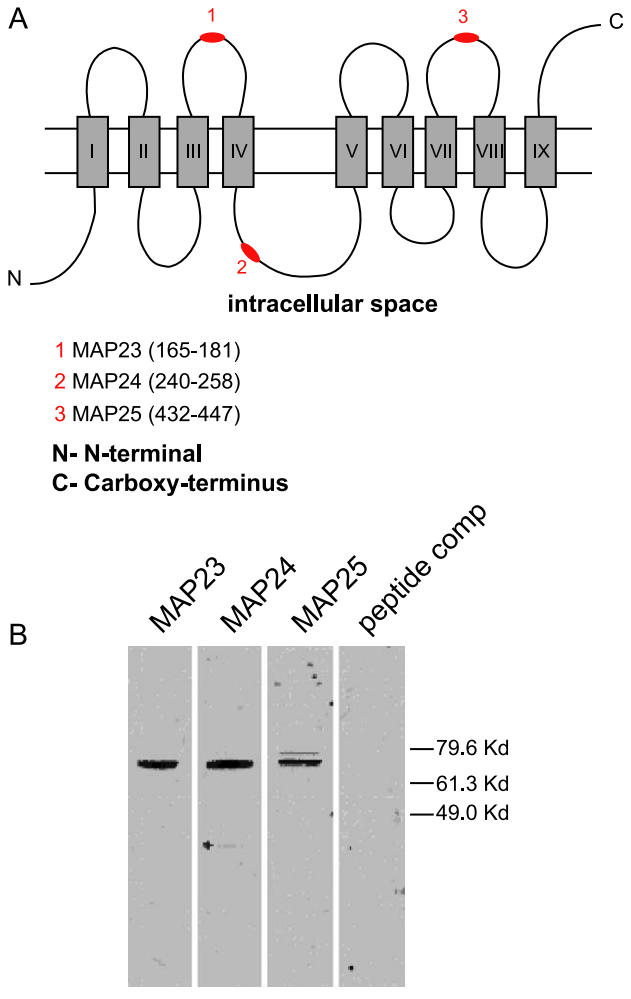

Fig. 1. (A) Antibodies to ferroportin peptides detect a single 62kD band. Predicted topology of ferroportin showing nine transmembrane domains and the position of peptides used to make antibodies as described in Materials and methods. Antibodies were raised against amino acid 165–181 (MAP 23), amino acids 240–258 (MAP 24), and against amino acids 432–447 (MAP25). (B) Western blot analysis using three different antibodies shows a major band around 62 kD. Fifty micrograms protein from brain lysate were used per lane. Lane 1: MAP 23, lane 2: MAP 24, lane 4: MAP 25, lane 4: negative control with excess MAP 24 peptide competition.

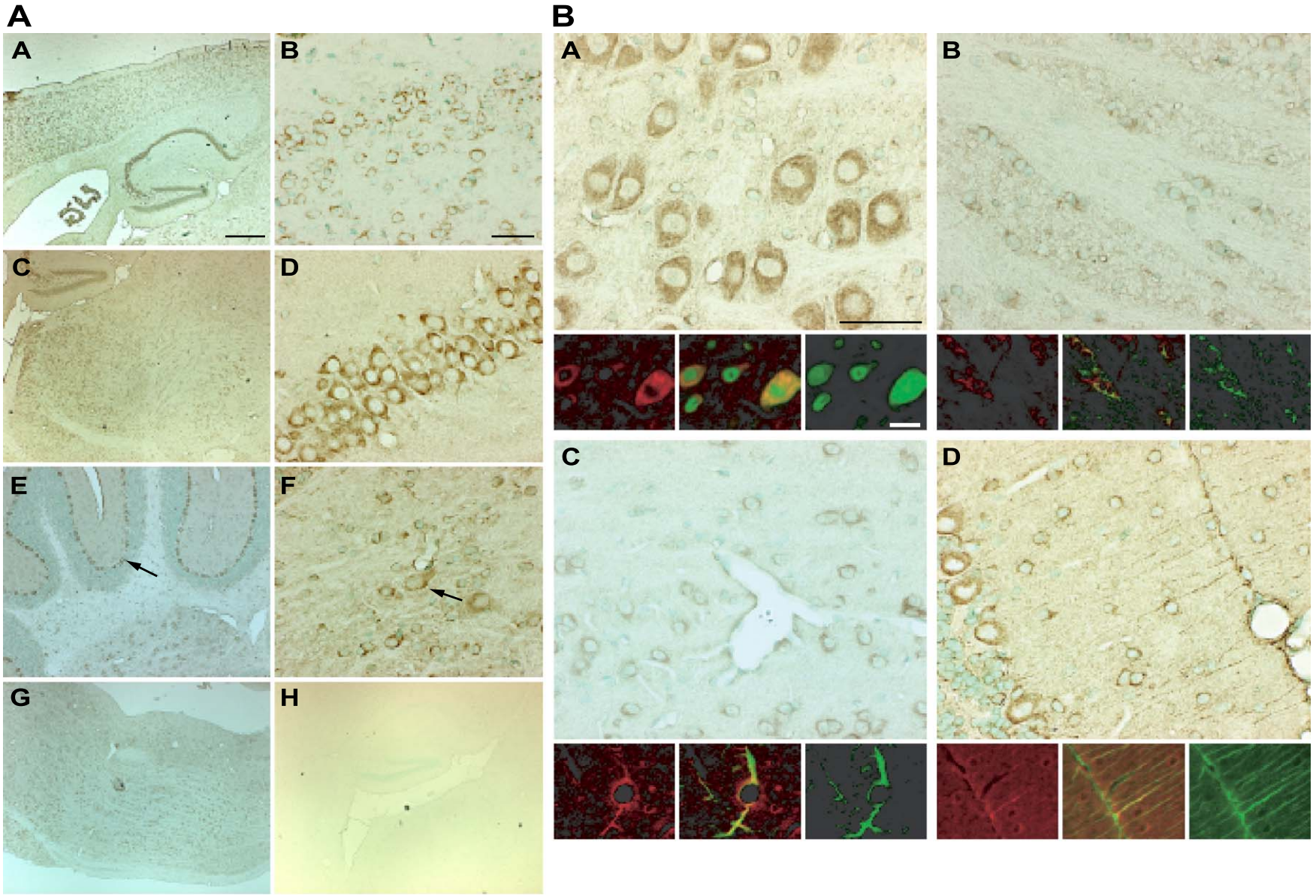

Fig. 2. A. Ferroportin detection by immunohistochemistry. (A) Ferroportin is found in neurons, oligodendrocytes and astrocytes. The staining of ferroportin is highest in the cortex (A, higher mag- B), thalamus (C), hippocampus (D), cerebellum (E), deep cerebellar nuclei (F) and brain stem (G), (40 ×, scale bar: 500 μm). Antibody to MAP 24 recognized neurons in the cortex (B), hippocampus (D) and cerebellar deep nucleus (F) (arrow, 600x, scale bar: 50 μm), Purkinje cells in the cerebellum (E, arrow), and oligodendrocytes in the cerebellar white matter (F, asterisk). Peptide competition (MAP 24 peptide) eliminated staining (H). B. Using fluorescent double staining, ferroportin staining is detected in neurons (A), oligodendrocytes (B), blood vessels (C) and Bergmann glia (D). Red represent the anti-ferroportin Ab, green represents either anti-Neu N, anti-CNPase, or anti-GFAP Ab, respectively. Scale bar: 50 and 20 μm (inset).

resulting suspension was layered over 5 ml of 1 M sucrose in medium L and centrifuged for 30 min at 96,300 × *g* in an SW27 rotor. The supernatant was mixed to homogeneity and centrifuged again for 14 h at 25,000 × *g*. The supernatant was collected as synaptic cytosol, and the pellets were homogenized in medium L, applied to a gradient of 7 ml 1.2, 1.0, 0.8, 0.6 and 0.4 M sucrose in medium L, and centrifuged for 90 min at 68,000 × *g* in an SW27 rotor. Bands at each interface were collected and washed once with medium L in a Ti50 rotor (45 min at 106,500 × *g*). The synaptic cytosol was dialyzed against medium L and centrifuged at 140,000 × *g* in a Ti 50 rotor for 1 h to separate any remaining synaptic vesicles from soluble proteins. All pellets were then resuspended in 20 mM Tris–HCl (pH 7.5). The concentrations of total proteins in each fraction were determined by BCA protein assay (PIERCE) against a BSA standard. Fractions were separated on 10–20% Tricine-SDS-PAGE, transferred to nitrocellulose membrane, and the membrane was sequentially immunoblotted with antibodies against ferroportin (MAP24, 1:1000), the plasma membrane marker Na^+/K^+ATPase (1:500, Transduction Labs), the synaptic vesicle

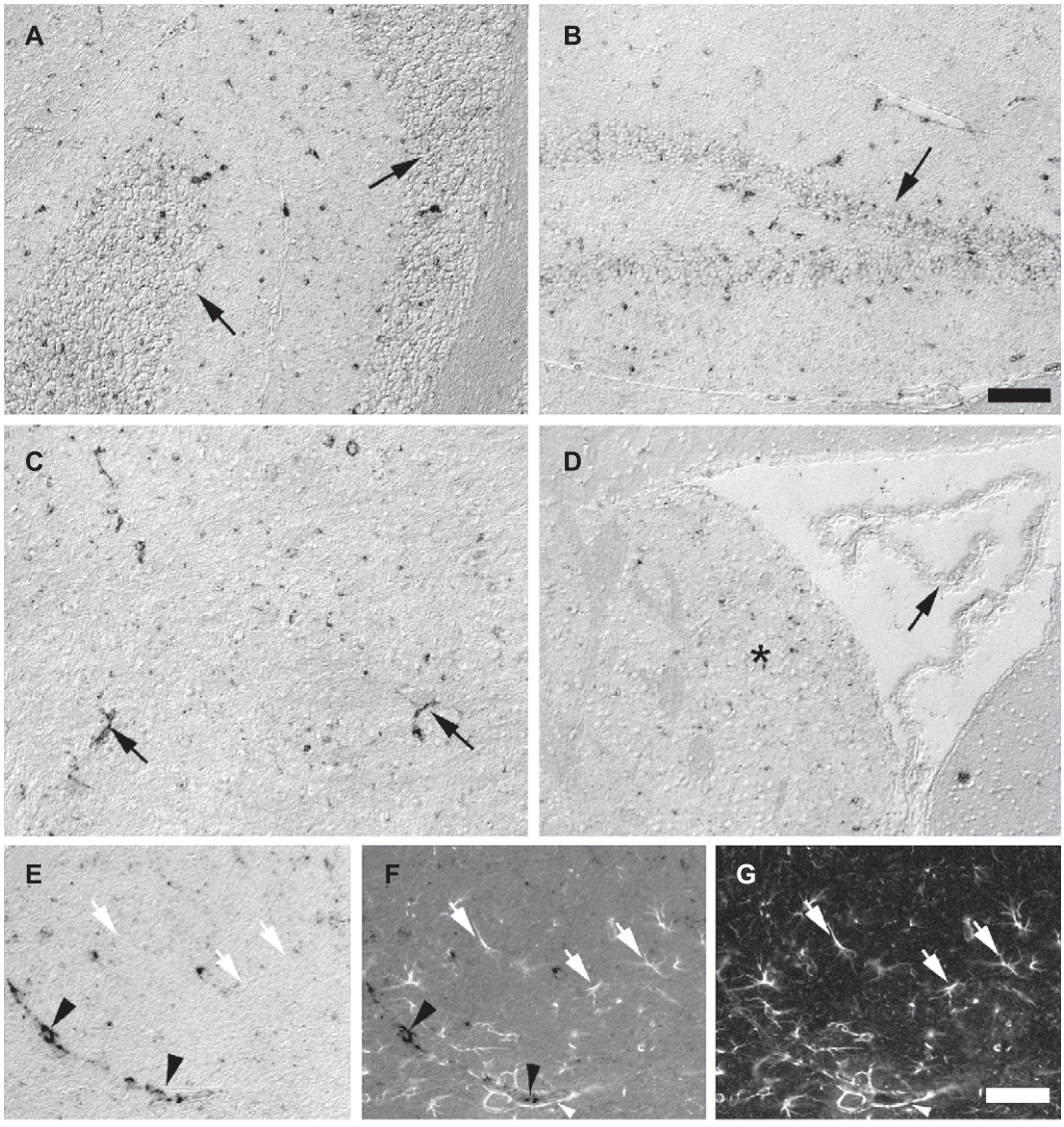

Fig. 3. In situ hybridization of ferroportin mRNA. Ferroportin message is found primarily in blood vessels throughout the brain including cerebellum (A), dentate gyrus (B), brainstem (C), striatum (asterisks) and choroid plexus (arrow) (D), and the molecular layer of the hippocampus (E, F, G). Bergmann glia (arrows in A) or choroid plexus (arrow in D) do not show ferroportin mRNA labeling. The dentate granule cells show only faint background labeling (arrow in B). Arrows in C point to transversely cut ferroportin-positive microcapillaries in brain stem. In (E), ferroportin mRNA labeling is shown in a section that was also processed for fluorescent GFAP staining (shown in G). The simultaneous view of ferroportin labeling and GFAP staining (F) demonstrates that astrocytes (white arrows) do not show detectable levels of ferroportin mRNA. Black arrowheads in (E), point to a blood vessel that is ferroportin positive, and that is enveloped by GFAP-positive astrocytic endfeet (white arrowhead). Size bar, A–D 100 μm (shown in B); E–F 50 μm.

marker synaptophysin (1:2000, Chemicon) and the cytosol marker β-tubulin (1:2000, Sigma).

Diet and iron dextran injection description: Newly weaned mice were maintained on a special diet containing either no added iron or normal mouse chow (Fe 0.2 gm/kg chow) from Harlan Teklad for a period of 8 weeks prior to sacrifice. Water was not iron-chelated. We know from prior experience with these diets that mice on the low iron diet develop signs of iron deficiency by eight weeks of age. To further address whether iron manipulations could affect brain ferroportin expression, we tried iron-loading mice with several different regimens of iron-dextran injection. These ranged from intraperitoneal injections of 20 mg iron dextran (100 mg/ml solution from Sigma), daily for 7 days (140 mg total), or for 14 days (280 mg total). Another pair of WT or IRP2 −/− mice was intraperitoneallly (i.p.) injected with 20 mg iron dextran daily for 3 days (a total of 60 mg iron dextran). A second pair was i.p. injected 20 mg daily for 6 days (120 mg). In a final set of experiments, we had two animals on the iron deficient diet for 9 months, two WT controls, and two animals that were injected with 2 mg iron dextran daily for five successive days. After all of these dietary manipulations, brain iron was stained with Perls'DAB stain, and iron overload was visibly achieved in all animals injected with iron dextran. Ferroportin immunohistochemistry was performed to see if ferroportin increases or decreases could be discerned at specific sites within the CNS on the low iron diet or in iron dextran injected animals.

3. Results

3.1. The distribution of ferroportin in neural cells

Antibodies against ferroportin peptides located on the extracellular (MAPs 23 and 25) or intracellular (MAP24) side of the membrane were used in Western blots of brain lysate (Fig. 1A,B). All three antibodies detected a band that migrated between the 61.3 and 79.6 kD markers. To determine the distribution of ferroportin in brain, affinity purified antibodies were used in immunohistochemistry experiments on paraformaldehyde-fixed, paraffin-embedded mouse brain sections. Ferroportin is widely expressed in brain, especially in the cortex, hippocampus, thalamus, brain stem and cerebellum (Fig. 2). Neuronal cell bodies showed strong positive staining throughout the brain. The immunoreactivity of oligodendrocytes was strong in white matter tracts, particularly in the brain stem and cerebellar white matter (F, asterisk). In the cerebellum, increased uniform staining was detected in the molecular layer whereas the staining was comparatively low in the granular layer (Fig. 2E). Purkinje cells expressed ferroportin, mostly in cell bodies and apical dendrites (Fig. 2E, arrow). Bergmann glia also expressed ferroportin. Peptide competition with MAP 24 demonstrated the specificity of ferroportin detection (Fig. 2H).

The identification of ferroportin in different cell types was confirmed by double-labeled immunoflurorescence using antibodies that recognized an oligodendrocyte specific marker (CNPase), a neuron specific marker (Neu N), or an astrocyte specific marker (GFAP) (Fig. 2B).

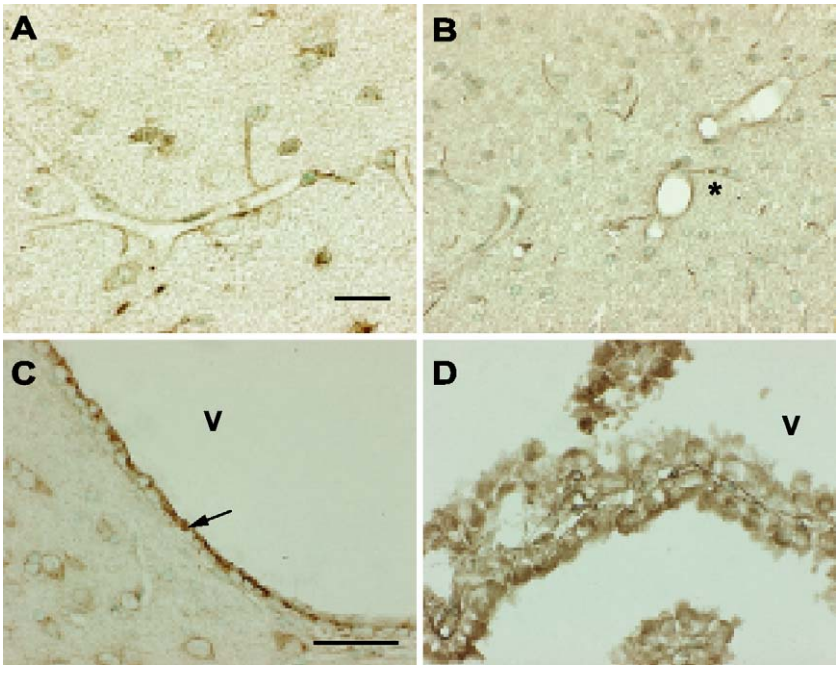

Fig. 4. Ferroportin protein is found in blood vessels, choroid plexus and ependymal cells. Ferroportin is located on the abluminal side of vessel walls (A) and the foot process of an astrocyte can be seen reaching to the blood vessel (B). Ferroportin is also detected in ependymal cells (C, arrow) and choroid plexus (D), where it is especially concentrated on the ventricular side (v).

To confirm our immunohistochemistry results, we performed in situ hybridization and detected ferroportin mRNA in cells throughout the brain. In the cerebellum, ferroportin labeling was detected in cells of the granular and molecular layers but not in the Bergmann glial layer (arrows, Fig. 3A). In the dentate gyrus (Fig. 3B), some ferroportin expressing cells were detected, but the granule cells only showed faint background labeling (arrow). The most prominent ferroportin labeling was present in short lines that were identified as microcapillaries (Fig. 3C). In addition, immunoreactive signals were detected in larger size blood vessels throughout the brain, particularly in the thalamus, striatum and cerebellum. Black arrowheads in panel E point to a ferroportin-positive blood vessel that is enveloped by GFAP-positive astrocytic endfeet (white arrowhead). Ferroportin mRNA was not detected in the choroid plexus or ependymal cells (Fig. 3D).

3.2. Ferroportin is expressed in the endothelial cells of the BBB

The primary function of the blood–brain-barrier (BBB) is to maintain a constant microenvironment for brain parenchyma. Transferrin receptors are present on the luminal side of the vascular endothelium to carry iron into the cells [18]. The iron transport mechanism across the abluminal membrane into brain parenchyma is not yet known. To determine whether ferroportin could be a candidate for this role, we examined its distribution within cells. Immunohistochemistry revealed that ferroportin was located mostly in blood vessel walls (Fig. 4A, B), particularly in the thalamus, striatum and cerebellum. Much of the ferroportin appeared to be concentrated on the abluminal side of vessel walls (Fig. 4B). The process of an astrocyte was immunostained by anti-ferroportin antibody and the foot process was clearly visible extending from the cell body to the blood vessels (Fig. 4B, asterisk). Ferroportin was also detected on the ventricular side of ependymal cells (Fig. 4C) and the choroid plexus (Fig. 4D).

3.3. Ferroportin is present in synaptic vesicles

We noted that ferroportin appeared to be localized in punctate dots that were not associated with cell bodies throughout the cerebellar molecular layer, cerebral cortex, striatum, thalamus and brain stem (Fig. 5A,B). However, ferroportin was not found in white matter tracts such as the corpus callosum and cerebellar white matter. To identify the punctate structures in which ferroportin was concentrated, we performed electron microscopy using pre-embedding immunohistochemistry and we discovered that ferroportin is associated with presynaptic vesicles (Fig. 4C–F). To confirm our ultrastructural identification of ferroportin in the presynaptic vesicles, we prepared a subcellular fractionation from crude synaptosomal prepa-

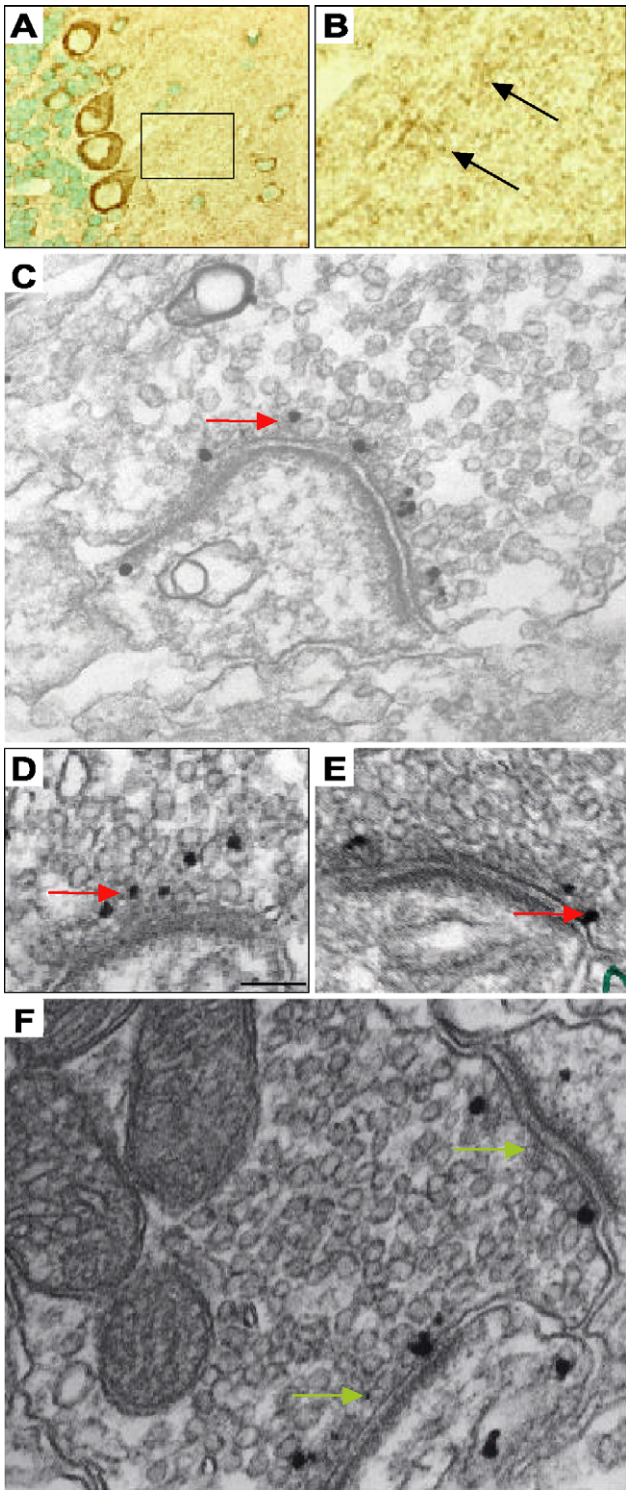

Fig. 5. (A) Ferroportin is present in synaptic vesicles. Ferroportin immunoreactivity is found in punctate spots along the dendrites of Purkinje cells and in the cerebellar molecular layer. (B) The punctate spots are more visible in a magnified view. (C–F) Using pre-embedding immunohistocytochemistry for electron microscopic studies, ferroportin is detected in presynaptic vesicles (black granules represent areas of ferroportin positivity. Arrows point to silver grains on pre-synaptic vesicles in C and D. Single synapses are shown in (C–E). A larger field containing two synapses (arrows) is shown in (F). Scale bar: 200 nm.

rations. By sucrose density gradient centrifugation, rat cerebral synaptosomes were fractionated into synaptic cytosol, synaptic vesicle, and synaptic plasma membrane fractions and then analyzed by sequential immunoblotting with various antibodies as indicated (Fig. 6). The relative purity of these subcellular fractions was confirmed by immunoreactivity corresponding to markers of synaptic vesicles (synaptophysin), plasma membrane (Na^+/K^+-ATPase), and cytosol (β-tubulin). Ferroportin was present predominantly in the synaptic vesicle fraction, consistent with our ultrastructural observations.

3.4. The expression level of ferroportin remains unchanged by iron overload or depletion

To determine whether ferroportin expression was detectably regulated by changes in systemic iron status, we performed immunohistochemistry, Northern blots and Western blots on animals maintained on a low iron diet after weaning compared to normal diet, and animals injected with iron dextran to produce iron overload (see Materials and methods). We also evaluated IRP2 −/− mice in which iron status was similarly manipulated, since ferroportin expression is markedly increased in the intestinal mucosa of IRP2 −/− mice [15]. However, we could not detect changes in ferroportin expression, either with immunohistochemistry (not shown), or in total brain lysates of WT or IRP2 −/− animals on low or normal iron diets by these measurements (Fig. 7), even though we could detect an increase in TfR mRNA levels in animals on the low iron diet (Fig. 7, bottom panel) indicating that the dietary iron restriction affected the brain. Notably, TfR expression is appropriately increased in the brain of WT animals on a low iron diet [18], but TfR levels are low and unregulated in IRP2 −/− mice, consistent with our previous observations that IRP2 is important for TfR transcript stabilization and regulation in animals [29,30].

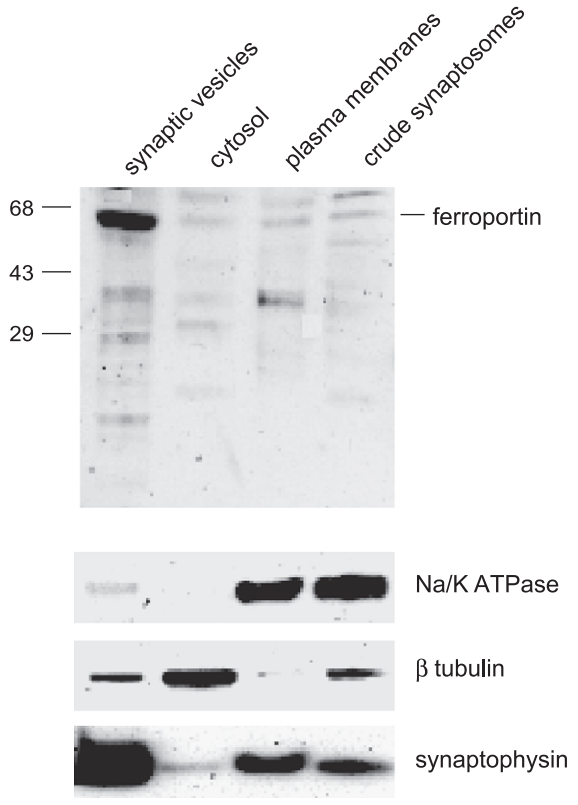

Fig. 6. Ferroportin is enriched in the synaptic vesicle fraction of purified synaptosomes. One microgram of rat brain synaptosome fractions enriched in synaptic cytosol, synaptic vesicles, and plasma membrane were analyzed by SDS-PAGE and sequentially immunoblotted with antibodies as indicated. Membranes were stripped and reprobed between applications of each antibody. The subcellular localization of ferroportin was determined by comparison with markers for synaptic vesicles (synaptophysin), plasma membrane (Na/K-ATPase), and cytosol (β-tubulin).

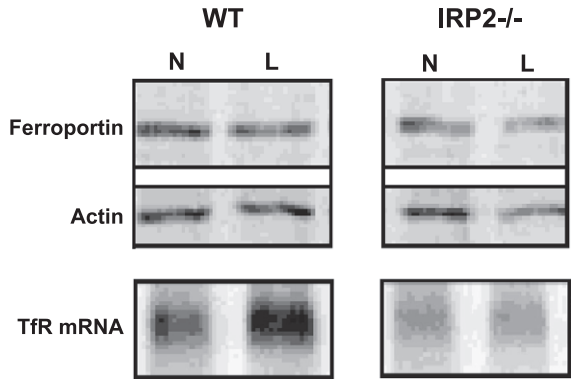

Fig. 7. Expression of ferroportin is not detectably affected by systemic iron status or loss of IRP2 activity. Ferroportin Western blotting was performed on brain lysates from WT or IRP2 −/− animals on a normal or low iron diet as described in materials and methods. Lysates were also probed with actin antibodies as a loading control. To assess CNS iron status and the effect of dietary manipulations, TfR mRNA levels were evaluated on Northern blots of total RNA prepared from these animals. Although TfR mRNA levels increased in WT animals on the iron-deficient diet, ferroportin protein levels did not change. TfR mRNA levels were low and unregulated in IRP2 −/− mice, in accordance with previous observations [21]. W/T: wild type, IRP2 −/− IRP2 knock-out , N: normal iron diet, L: iron deficient diet.

4. Discussion

Our studies have revealed that ferroportin is widely expressed throughout the brain. Immunohistochemical analysis showed ferroportin expression by several cell types including neurons, astrocytes, endothelial cells of blood vessels, and epithelial cells of the choroid plexus, whereas ferroportin mRNA was detected by in situ hybridization analysis only in blood vessels. This apparent discrepancy is likely attributable to the limited detection sensitivity of non-isotopic in situ hybridization. However, the in situ hybridization results substantiated the immunohistochemical detection of ferroportin in blood vessels, an important site for understanding brain iron homeostasis.

Immunohistochemistry revealed that ferroportin is expressed at regions in which tissues interface with blood or cerebrospinal fluid, including blood vessel walls, choroid plexus, and ependymal cells. Iron is generally believed to enter the brain by transport across the blood vessel endothelial cells that form the blood–brain barrier. After uptake of transferrin-bound iron, iron dissociates from transferrin and enters the brain parenchyma by an unknown mechanism [18]. Our observation that ferroportin appears more concentrated on the abluminal side of blood vessels implies that iron can be transported from blood stream to brain tissue. The expression of ferroportin in astrocytic foot processes further suggests a critical role of ferroportin in brain iron uptake across the BBB.

Although it is known that choroid plexus epithelial cells contain transferrin receptor, iron, and ferritin, the role of the choroid plexus in regulating iron availability to the CSF has not been investigated extensively. The localization of ferroportin on the ventricular side of ependymal cells and the choroid plexus suggests that ferroportin exports iron from the brain parenchyma and circulation into cerebro-spinal fluid, which ultimately reenters the systemic circulation.

Ferroportin mRNA contains an iron-responsive element in its 5′ UTR, and the IRE has been previously shown to confer regulation of ferroportin expression according to iron status by IRPs [17]. We have previously observed increased ferroportin expression in the intestinal mucosa of IRP2 −/− mice [21]. However, Western and Northern blots indicate that there is no significant difference in ferroportin expression in the brain in animals on a low-iron diet, even though an increase in transferrin receptor expression can be shown under the same conditions. Thus, although regulation of ferroportin expression in the blood–brain barrier and choroid plexus could offer a potential mechanism for regulating entry of iron into the CNS, we find no evidence that such regulation takes place. It remains possible that ferroportin is regulated at specific sites that are important in brain iron homeostasis, but our techniques may be insufficiently sensitive to detect regulation in a small population of cells.

An unexpected and interesting outcome of our work is that presynaptic vesicles contain ferroportin. This discovery implies that iron is transported from cytosol into vesicles in the synaptic cleft and that ferrous iron could be released into the synaptic cleft upon vesicle fusion. The presence of free iron in the synapse could potentially expose the pre- and post-synaptic membranes to iron-dependent oxidation and damage. The specificity of ferroportin in metal transport has not been experimentally determined. However, specificity studies of the related metal importer DMT1 reveal that DMT1 transports manganese, cadmium and cobalt efficiently [12]. Manganese is believed to undergo axonal transport and to be concentrated in the synaptic vesicles of glutamatergic cells [26]. It is therefore theoretically possible that the ferroportin detected in synaptic vesicles is there for the purpose of transporting manganese. There is no known or postulated role for iron in synaptic vesicles at this time. However, the presence of ferroportin in synaptic vesicles implies that axonal free iron can be exported to the synaptic cleft and then be taken up by astrocytes or post-synaptic neurons. These discoveries imply that intracellular iron trafficking within the CNS may represent an important mechanism for moving iron from one location to another. Moreover, abnormalities in iron homeostasis may have a direct adverse effect on synaptic integrity.

Acknowledgements

The authors thank the Electron Microscopic Imaging Core Facility of NINDS for their help.

References

[1] S. Abboud, D.J. Haile, A novel mammalian iron-regulated protein involved in intracellular iron metabolism, J. Biol. Chem. 275 (2000) 19906–19912.
[2] G.J. Anderson, D.M. Frazer, A.T. McKie, S.J. Wilkins, C.D. Vulpe, The expression and regulation of the iron transport molecules hephaestin and IREG1: implications for the control of iron export from the small intestine, Cell Biochem. Biophys. 36 (2002) 137–146.
[3] D. Berg, M. Gerlach, M.B. Youdim, et al., Brain iron pathways and their relevance to Parkinson's disease, J. Neurochem. 79 (2001) 225–236.
[4] U.V. Berger, M.A. Hediger, Comparative analysis of glutamate transporter expression in rat brain using differential double in situ hybridization, Anat. Embryol. (Berl). 198 (1998) 13–30.
[5] J.R. Burdo, S.L. Menzies, I.A. Simpson, et al., Distribution of divalent metal transporter 1 and metal transport protein 1 in the normal and Belgrade rat, J. Neurosci. Res. 66 (2001) 1198–1207.
[6] F. Canonne-Hergaux, S. Gruenheid, P. Ponka, P. Gros, Cellular and subcellular localization of the Nramp2 iron transporter in the intestinal brush border and regulation by dietary iron, Blood 93 (1999) 4406–4417.
[7] J.R. Connor, G. Pavlick, D. Karli, S.L. Menzies, C. Palmer, A histochemical study of iron-positive cells in the developing rat brain, J. Comp. Neurol. 355 (1995) 111–123.
[8] D.W. Dickson, W. Lin, W.K. Liu, S.H. Yen, Multiple system atrophy: a sporadic synucleinopathy, Brain Pathol. 9 (1999) 721–732.
[9] A. Donovan, A. Brownlie, Y. Zhou, et al., Positional cloning of zebrafish ferroportin1 identifies a conserved vertebrate iron exporter, Nature 403 (2000) 776–781.
[10] P.R. Dunkley, J.W. Heath, S.M. Harrison, P.E. Jarvie, P.J. Glenfield, J.A. Rostas, A rapid Percoll gradient procedure for isolation of synaptosomes directly from an S1 fraction: homogeneity and morphology of subcellular fractions, Brain Res. 441 (1988) 59–71.
[11] N. Gordon, Iron deficiency and the intellect, Brain Develop. 25 (2003) 3–8.
[12] H. Gunshin, B. Mackenzie, U.V. Berger, et al., Cloning and characterization of a mammalian proton-coupled metal-ion transporter, Nature 388 (1997) 482–488.
[13] S.J. Hayflick, Pantothenate kinase-associated neurodegeneration (formerly Hallervorden-Spatz syndrome), J. Neurol. Sci. 207 (2003) 106–107.
[14] G. Lao, V. Scheuss, C.M. Gerwin, et al., Syntaphilin: a syntaxin-1 clamp that controls SNARE assembly, Neuron. 25 (2000) 191–201.
[15] T. LaVaute, S. Smith, S. Cooperman, et al., Targeted deletion of iron regulatory protein 2 causes misregulation of iron metabolism and neurodegenerative disease in mice, Nat. Genet. 27 (2001) 209–214.
[16] D. Li, Effects of iron deficiency on iron distribution and gamma-

aminobutyric acid (GABA) metabolism in young rat brain tissues, Hokkaido Igaku Zasshi 73 (1998) 215–225.
[17] W.R. Martin, F.Q. Ye, P.S. Allen, Increasing striatal iron content associated with normal aging, Mov. Disord. 13 (1998) 281–286.
[18] T. Moos, E.H. Morgan, Transferrin and transferrin receptor function in brain barrier systems, Cell. Mol. Neurobiol. 20 (2000) 77–95.
[19] C.P. Ponting, Domain homologues of dopamine beta-hydroxylase and ferric reductase: roles for iron metabolism in neurodegenerative disorders? Hum. Mol. Genet. 10 (2001) 1853–1858.
[20] T.A. Rouault, Systemic iron metabolism: a review and implications for brain iron metabolism, Pediatr. Neurol. 25 (2001) 130–137.
[21] T. Rouault, R. Klausner, Regulation of iron metabolism in eukaryotes, Curr. Top. Cell. Regul. 35 (1997) 1–19.
[22] B.D. Schneider, E.A. Leibold, Regulation of mammalian iron homeostasis, Curr. Opin. Clin. Nutr. Metab. Care 3 (2000) 267–273.
[23] Z.H. Sheng, J. Rettig, T. Cook, W.A. Catterall, Calcium-dependent interaction of N-type calcium channels with the synaptic core complex, Nature 379 (1996) 451–454.
[24] M.A. Smith, P.L. Harris, L.M. Sayre, G. Perry, Iron accumulation in Alzheimer disease is a source of redox-generated free radicals, Proc. Natl. Acad. Sci. U. S. A. 94 (1997) 9866–9868.
[25] M. Takanashi, H. Mochizuki, K. Yokomizo, et al., Iron accumulation in the substantia nigra of autosomal recessive juvenile parkinsonism, Parkinsonism Relat. Disord. 7 (2001) 311–314.
[26] A. Takeda, Manganese action in brain function, Brain Res. Brain Res. Rev. 41 (2003) 79–87.
[27] J.P. Tam, Synthetic peptide vaccine design: synthesis and properties of a high-density multiple antigenic peptide system, Proc. Natl. Acad. Sci. 85 (1988) 5409–5413.
[28] R.B. Wilson, Frataxin and frataxin deficiency in Friedreich's ataxia, J. Neurol. Sci. 207 (2003) 103–105.
[29] E.G. Meyron-Holtz, M.C. Ghosh, K. Iwai, T. Lavaute, X. Brazzolotto, U. Berger, W. Land, H. Ollivierre-Wilson, A. Grinberg, P. Love, T.A. Rouault, Genetic ablations of iron regulatory proteins 1 and 2 reveal why iron regulatory protein 2 dominates iron homeostasis, EMBO J., in press.
[30] S.R. Smith, S. Cooperman, T. Lavaute, N. Tresser, M. Ghosh, E. Meyron-Holtz, W. Land, H. Ollivierre, B. Jortner, R. Switzer, A. Messing, T.A. Rouault, Severity of neurodegeneration correlates with compromise of iron metabolism in mice with iron regulatory protein deficiencies, Ann. N.Y. Acad. Sci., in press.